The Astrophysical Journal, 635:86–99, 2005 December 10

QUANTITATIVE SIGNATURES OF GALACTIC SUPERWINDS ON Lyα CLOUDS AND METAL-LINE SYSTEMS

Renyue Cen,[1] Kentaro Nagamine,[2] and Jeremiah P. Ostriker[3]

Received 2004 July 7; accepted 2005 August 15

ABSTRACT

We investigate possible signatures of feedback from galactic superwinds (GSWs) on the metallicity of the Lyα forest, using a set of high-resolution hydrodynamic simulations of a ΛCDM model. Simulations produce metals self-consistently, based on one single parameter, the metal yield, which in turn is constrained by metallicity in the intracluster gas. We follow metals as a separate density species. The metallicity of Lyα clouds having column density of $N_{\rm H\,I}\sim10^{14.5}$–$10^{15.5}$ cm^{-2} at $z=2$–4 is correctly predicted by simulations, both with and without GSWs, implying an in situ origin for these metals. However, a unique signature and sensitive test of GSWs are provided by lower column density clouds of 10^{12}–10^{14} cm^{-2}. We find that the number density of Lyα lines with metallicity $Z\geq10^{-3}$ $Z_\odot$ and neutral hydrogen column density $N_{\rm H\,I}<10^{13.5}$ cm^{-2} provides a first quantitative measure of the strength of GSWs, because metals in these systems are a contaminant. We predict that the number of such lines per unit redshift at $z\sim3$ should be about 0.1 in the absence of GSWs. With the observed GSW strength, we expect to see 20–50 such lines per unit redshift. This is an observational challenge. Furthermore, we find that the difference between simulations with and without GSWs becomes much larger with regard to a subset of such clouds with high Doppler widths, since the contaminated systems are considerably hotter than the normal IGM. We also present preliminary results on C IV and O VI lines as a function of GSW strength. The filling factor of metal-rich regions is a strong function of GSWs. With and without GSWs the volume filling factor is 6.0%, 4.2%, and 1.9% and 1.0%, 0.28%, and 0.08%, respectively, for regions with metallicity greater than 10^{-3}, 10^{-2}, and 10^{-1} $Z_\odot$. Finally, in clouds of $N_{\rm H\,I}\sim10^{14.5}$ cm^{-2}, we predict that the ratio of secondary (e.g., N) to primary metals (e.g., O, C) is expected to be smaller by a factor of 10 than in large galaxies, which better retain metals; this factor increases to $\geq$50 for $N_{\rm H\,I}\leq10^{13.5}$ cm^{-2}.

Subject headings: cosmology: theory — hydrodynamics — intergalactic medium — large-scale structure of universe — quasars: absorption lines

Online material: color figures

1. INTRODUCTION

Direct observational evidence for feedback from galactic superwinds (GSWs) originating in starburst galaxies is ubiquitous both at low redshift (e.g., McCarthy et al. 1987; Heckman et al. 1987, 1998; Papaderos et al. 1994; Marlowe et al. 1995; Lehnert & Heckman 1996; Bland & Tully 1988; Filippenko & Sargent 1992; Dahlem et al. 1998; Martin 1999; Yoshida et al. 1999; Veilleux et al. 1999, 2001; Della Ceca et al. 1999; Rupke et al. 2002; Martin et al. 2002) and at high redshift (e.g., Franx et al. 1997; Pettini et al. 1998, 2001, 2002; Dawson et al. 2002; Adelberger 2003; Adelberger et al. 2003). In addition, two lines of indirect but independent observational evidence point to the existence of or need for GSWs. First, the low- to moderate-density regions of the intergalactic medium (IGM) in Lyα clouds at $z\sim2$–3 have already been enriched with metals to significant levels (e.g., Tytler et al. 1995; Songaila & Cowie 1996; Bergeron et al. 2002) to a level that would be difficult to achieve by sources embedded in those regions. And in the warm-hot intergalactic medium at low redshift (e.g., Tripp et al. 2000; Fang et al. 2002; Nicastro et al. 2002; Mathur et al. 2003) metals are seen that presumably originate from the galaxies central to these regions. Second, a substantial, nongravitational heating source of the intracluster medium may be needed to produce the observed X-ray cluster luminosity-temperature relation and its evolution (e.g., Kaiser 1991; White 1991; David et al. 1991; Metzler & Evrard 1994; Navarro et al. 1995; Pen 1999; Ponman et al. 1999; Balogh et al. 1999; Loewenstein 2000; Wu et al. 2000; Lloyd-Davies et al. 2000; Brighenti & Mathews 2001; Neumann & Arnaud 2001; Borgani et al. 2001; Voit & Bryan 2001; Tozzi & Norman 2001; Davé et al. 2001; Babul et al. 2002; Bialek et al. 2001; McCarthy et al. 2002; Afshordi & Cen 2002; Voit et al. 2002). GSWs may play a significant role in the transport of metal-enriched matter to lower density regions outside galaxies and may help provide the requisite nongravitational heating source for the cluster gas.

In contrast to notable successes of cosmological hydrodynamic simulations of the IGM that has not been intimately involved in star formation, such as the Lyα forest (Cen et al. 1994; Zhang et al. 1995; Hernquist et al. 1996; Miralda-Escudé et al. 1996; Bond & Wadsley 1998; Theuns et al. 1998), few calculations have been made to investigate the impact of GSWs on the IGM in a coherent fashion. So far, most brute-force cosmological hydrodynamic simulations do not include the feedback effects of the GSWs. For those simulations with GSWs included (Cen & Ostriker 1992, 1993, 1999a, 1999b; Cen et al. 1994; Gnedin & Ostriker 1997; Gnedin 1998; Springel & Hernquist 2003; Kay et al. 2002; Theuns et al. 2002), the obtained results are often paradoxical; for example, in very high resolution simulations dense regions tend to radiate away most of the GSW feedback energy and thus largely suppress its effect. This is for the most part due to the limited (and sometimes mismatched spatial and

[1] Princeton University Observatory, Princeton University, Princeton, NJ 08544; cen@astro.princeton.edu.

[2] Harvard-Smithsonian Center for Astrophysics, 60 Garden Street, Cambridge, MA 02138; knagamin@cfa.harvard.edu.

[3] Princeton University Observatory, Princeton University, Princeton, NJ 08544; jpo@astro.princeton.edu.

mass) numerical resolutions with the inability to properly represent, in cosmological simulations, a multiphase ISM, where a GSW originates. On the other hand, simulations with lower resolution, limited by available computer power, but with a crude multiphase medium treatment (e.g., Cen & Ostriker 1999a, 1999b) appear to be able to exert substantial feedback energy on the general IGM surrounding galaxies. But the very limited resolution of these simulations does not allow us to draw reliable quantitative conclusions.

Although it is generally accepted that energy from collective supernova (SN) explosions and stellar winds should be powering the GSWs (Ostriker & Cowie 1981; Dekel & Silk 1986; see Aguirre 1999 for a study of the role radiation pressure on dust plays in driving outflows), the complex structure of the interstellar medium (ISM; McKee & Ostriker 1977) and the IGM makes quantitative calculations of GSWs and their subsequent evolution a daunting task, which certainly requires treatment of a multiphase medium and may necessitate the explicit inclusion of magnetic fields (Koo & McKee 1992a, 1992b; Smith 1996; Suchkov et al. 1996; Nath & Trentham 1997; Hartquist et al. 1997; Gnedin & Ostriker 1997; Gnedin 1998; Mac Low & Ferrara 1999; Cen & Ostriker 1999b; Ferrara et al. 2000; Madau et al. 2001; Aguirre et al. 2001; Mori et al. 2002; Scannapieco et al. 2001, 2002; Thacker et al. 2002; White et al. 2002; Dyson et al. 2002; Springel & Hernquist 2003). Significant progress has been made recently to provide a better treatment of the multiphase ISM (Yepes et al. 1997; Elizondo et al. 1999a, 1999b; Hultman & Pharasyn 1999; Ritchie & Thomas 2001; Springel & Hernquist 2003), but the generation of GSWs is far from being adequately modeled. Clearly, a combination of both high resolution and detailed multiphase medium treatment (including magnetic fields and cosmic rays) is needed before our understanding of the interactions between galaxy formation and the IGM can be considered to be truly satisfactory.

But we follow a somewhat different approach. We do not attempt to model the complex physics which determines how much of the SN energy produced within the galaxies can escape the galaxies. Rather, we inject energy directly into the medium surrounding the galaxies in a fashion that drives GSWs and we adjust the energy input to match the observed GSWs (e.g., Pettini et al. 2001, 2002; Heckman 2001). Direct and empirical determination of the output of energy and metal-enriched gas from GSWs is, in principle, possible (Chevalier & Clegg 1985), although, in practice, a complete account of the energy and mass output (especially the hot component at the X-ray band) from GSWs may require more involved work (Strickland & Stevens 2000). Nevertheless, direct observational determinations of mass- and energy-loss rates from GSWs have yielded very interesting results (see Heckman 2001 for a recent review), with observations of both low-redshift starburst galaxies and high-redshift Lyman break galaxies (LBGs) indicating that both mass and energy outflows from GSWs are comparable to those supplied by the interior starburst.

Thus, we accept at the outset our inability to correctly model the detailed structure of the ISM within these galaxies or the *generation* of the GSWs. Rather, we simply assume a proportionality between the star formation rate $\dot{M}_*$ in the system and the output by that system of wind mass flux and energy flux, since there is a sound observational basis for this assumption. So we assume that the energy *output* in a GSW is related to the star formation rate by $\dot{E}_{\rm GSW} = e_{\rm GSW} c^2 \dot{M}_*$ (where c is the speed of light) and that the mass output is $\dot{M}_{\rm GSW} = e_{\rm mass} \dot{M}_*$. The two adjustable parameters ($e_{\rm GSW}$ and $\beta_{\rm GSW}$) are then determined by a fit to observations (e.g., Pettini et al. 2001, 2002; Heckman 2001), specifically, the two observed parameters—the mass flow rate and the wind velocity—and our subsequent computations are used to determine the *effects* of the consequent GSWs on the metallicity distribution within the IGM, the shock-heating input to the IGM, and the modification/regulation of subsequent galaxy formation. In brief, we seek to model the consequences, not the causes, of GSW feedback, and this is something that we think our codes are well designed to do. It should be stated that our approach, since it is a phenomenological one, is clearly incapable of fully solving the feedback process. But this is a major step toward understanding the effects of GSWs, given the current state of knowledge, which leaves the physics of generation of GSW largely unconstrained.

It may be useful to put this in a historical context. A decade ago the focus of cosmological simulations (e.g., Cen et al. 1994) was to fit the observed Lyα forest into the picture of modern hierarchical structure formation theory. The result was the emergence of the now standard theory for Lyα forest based on the growth/collapse of small-scale density perturbations at moderate redshift. In this post-*WMAP* (*Wilkinson Microwave Anisotropy Probe*) era, the research focus for the Lyα forest has become to provide answers to the following questions: how does galaxy formation affect the properties of Lyα forest and how is the power spectrum of primordial density fluctuation on small scales reconstructed from Lyα forest flux distribution subject to various processes related to galaxy formation? This paper attempts to provide some partial answers to the first question. In this first of a series of papers focusing on the effects of GSWs on the IGM and subsequent galaxy/star formation, we investigate the effect of GSW on the metal enrichment of the Lyα forest at high redshift ($z = 2$–4), which contains most of the mass as well as volume of the IGM at that time. The outline of this paper is as follows. The simulation details are given in § 2. In § 3 we give detailed results, and we conclude in § 4.

2. SIMULATIONS

Numerical methods of the cosmological hydrodynamic code and input physical ingredients have been described in detail in an earlier paper (Cen et al. 2003). We name the code TIGER (derived from TVD [total variation diminishing] for intergalactic medium and galaxy evolution and formation). Briefly, the simulation integrates five sets of equations simultaneously: the Euler equations for gas dynamics, rate equations for different hydrogen and helium species at different ionization states, the Newton equations of motion for dynamics of collisionless particles, the Poisson equation for obtaining the gravitational potential field, and the equation governing the evolution of the intergalactic ionizing radiation field—all in cosmological comoving coordinates. Note that the cosmological (frequency dependent) radiation field is solved for self-consistently, rather than being a separate input to the modeling. The gasdynamical equations are solved using the TVD shock-capturing code (Ryu et al. 1993) on an uniform mesh. The rate equations are treated using subcycles within a hydrodynamic time step due to much shorter ionization timescales (i.e., the rate equations are very "stiff"). Dark matter particles are advanced in time using the standard particle-mesh (PM) scheme. The gravitational potential on an uniform mesh is solved using the fast Fourier transform (FFT) method.

The initial conditions adopted are those for Gaussian processes with the phases of the different waves being random and uncorrelated. The initial condition is generated by the COSMICS software package kindly provided by E. Bertschinger (2001).

Cooling and heating processes due to all the principal line and continuum atomic processes for a plasma of primordial

composition with additional metals ejected from star formation (see below), Compton cooling due to the microwave background radiation field, and Compton cooling/heating due to the X-ray and high-energy background are computed in a time-dependent, nonequilibrium fashion. The cooling due to metals is computed using a code based on the Raymond-Smith code (Raymond et al. 1976) assuming ionization equilibrium (Cen et al. 1995).

We follow star formation using a well-defined prescription used by us in our earlier work (Cen & Ostriker 1992, 1993) and similar to that of other investigators (Katz et al. 1992, 1996; Steinmetz 1996; Gnedin & Ostriker 1997). A stellar particle of mass $m_* = c_* m_{\rm gas} \Delta t/t_*$ is created (the same amount is removed from the gas mass in the cell), if the gas in a cell at any time meets the following three conditions simultaneously: (1) contracting flow, (2) cooling time less than dynamic time, and (3) Jeans unstable, where Δt is the time step, $t_* = \max(t_{\rm dyn},\ 10^7\ {\rm yr})$, $t_{\rm dyn} = [3\pi/(32 G\rho_{\rm tot})]^{1/2}$ is the dynamical time of the cell, $m_{\rm gas}$ is the baryonic gas mass in the cell, and $c_* = 0.07$ is star formation efficiency.

Each stellar particle has a number of other attributes at birth, including formation time t_i, initial gas metallicity, and the free-fall time in the birth cell $t_{\rm dyn}$. The typical mass of a stellar particle in the simulation is about a million solar masses; in other words, these stellar particles are like coeval globular clusters.

Stellar particles are subsequently treated dynamically as collisionless particles. But feedback from star formation is allowed in three forms: ionizing UV photons, supernova kinetic energy (i.e., GSWs), and metal-enriched gas, all being proportional to the local star formation rate. The temporal release of all three feedback components at time t has the same form: $f(t,\ t_i,\ t_{\rm dyn}) \equiv (1/t_{\rm dyn})[(t-t_i)/t_{\rm dyn}] \exp[-(t-t_i)/t_{\rm dyn}]$. Within a time step dt, the released GSW energy to the IGM, ejected mass from stars into the IGM, and escape UV radiation energy are $e_{\rm GSW} f(t,\ t_i,\ t_{\rm dyn}) m_* c^2 dt$, $e_{\rm mass} f(t,\ t_i,\ t_{\rm dyn}) m_* dt$, and $f_{\rm esc}(Z) e_{\rm UV}(Z) f(t,\ t_i,\ t_{\rm dyn}) m_* c^2 dt$. We use the Bruzual-Charlot population synthesis code (Bruzual & Charlot 1993; Bruzual 2000) to compute the intrinsic metallicity-dependent UV spectra from stars with a Salpeter initial mass function (IMF; with a lower and upper mass cutoff of 0.1 and 125 $M_\odot$). Note that $e_{\rm UV}$ is no longer just a simple coefficient but a function of metallicity. The Bruzual-Charlot code gives $e_{\rm UV} = (1.2\times10^{-4},\ 9.7\times10^{-5},\ 8.2\times10^{-5},\ 7.0\times10^{-5},\ 5.6\times10^{-5},\ 3.9\times10^{-5},\ 1.6\times10^{-6})$ at $Z/Z_\odot = (5.0\times10^{-3},\ 2.0\times10^{-2},\ 2.0\times10^{-1},\ 4.0\times10^{-1},\ 1.0,\ 2.5,\ 5.0)$. We also implement a gas metallicity–dependent ionizing photon escape fraction from galaxies in the sense that higher metallicity, and hence higher dust content, galaxies are assumed to allow a lower escape fraction; we adopt the escape fractions of $f_{\rm esc} = 2\%$ and 5% (Hurwitz et al. 1997; Deharveng et al. 2001; Heckman et al. 2001) for solar and $\frac{1}{10}$ of solar metallicity, respectively, and interpolate/extrapolate using a linear log form of metallicity. In addition, we include the emission from quasars using the spectral form observationally derived by Sazonov et al. (2004), with a radiative efficiency in terms of stellar mass of $e_{\rm QSO} = 2.5\times10^{-5}$ for $h\nu > 13.6$ eV. Finally, hot, shocked regions (such as clusters of galaxies) emit ionizing photons due to bremsstrahlung radiation, which are also included. The UV component is simply averaged over the box, since the light propagation time across our box is small compared to the time steps. The radiation field (from 1 eV to 100 keV) is followed in detail with allowance for self-consistently produced radiation sources and sinks in the simulation box and for cosmological effects, i.e., radiation transfer for the mean field J_ν is computed with stellar, quasar, and bremsstrahlung sources and sinks due to Lyα clouds, etc. In addition, a local optical depth approximation is adopted to crudely mimic the local shielding effects: each cubic cell is flagged with six hydrogen "optical depths" on the six faces, each equal to the product of neutral hydrogen density, hydrogen ionization cross section, and scale height, and the appropriate mean from the six values is then calculated; equivalent ones for neutral helium and singly ionized helium are also computed. In computing the global sink terms for the radiation field the contribution of each cell is subject to the shielding due to its own "optical depth." In addition, in computing the local ionization and cooling/heating balance for each cell, the same shielding is taken into account to attenuate the external ionizing radiation field.

GSW energy and ejected metals are distributed into 27 local gas cells centered at the stellar particle in question, weighted by the specific volume of each cell. We fix $e_{\rm mass} = 0.25$. GSW energy injected into the IGM is included with an adjustable efficiency (in terms of the rest-mass energy of the total of formed stars) of $e_{\rm GSW}$, which is normalized to observations for our fiducial simulation with $e_{\rm GSW} = 3\times10^{-6}$. If the ejected mass and associated energy propagate into a vacuum, the resulting velocity of the ejecta would be $(e_{\rm GSW}/e_{\rm mass})^{1/2} c = 1469\ {\rm km\ s^{-1}}$. After the ejecta has accumulated an amount of mass comparable to its initial mass, the velocity may slow down to a few hundred kilometers per second. We assume this velocity would roughly correspond to the observed outflow velocities of LBGs (e.g., Pettini et al. 2002). We also make simulations with no GSWs and with stronger GSWs to investigate the effects of GSWs on the IGM.

We do not separately make any adjustments to fit to the observed distributions and evolution of metals, but assume a specific efficiency of metal formation, a "yield" (Arnett 1996), $y_0 = 0.02$, the percentage of stellar mass that is ejected back into the IGM as metals. We note that $y_0 = Z_{\rm ejecta} e_{\rm mass}$; since $y_0 = 0.02$ and $e_{\rm mass} = 0.25$, it implies that the ejecta metallicity is $Z_{\rm ejecta} = 0.08 = 4\ Z_\odot$. Metals in the IGM (assuming the standard solar composition) are followed as a separate variable (analogous to the total gas density) with the same hydrocode. In addition, we implement another density variable to keep track of the reprocessed, i.e., secondary metals in the ejecta, which is proportional to the metallicity of the gas from which the star was formed.

Since we are interested in the metallicity of the IGM, it is legitimate to question whether our adopted constant metal yield is reasonable. We cannot answer this question from first principles. Rather, we consider a physically motivated case, in which the metallicity yield is a function of the gas metallicity from which stars are formed. It is thought that the IMF of stars formed out of low-metallicity gas may contain relatively more high-mass stars and thus produce a higher yield (for references to the original literature, see Ricotti & Ostriker 2004). We adopt this view and consider a scenario with varying yield by making a correction to the computed yield as described below. We present results for both the case of constant yield and metallicity-dependent yield to indicate the uncertainties and/or adjustability of the results.

Let the yield be $y(Z)$. It can then be shown that the final corrected metallicity of a region with computed metallicity Z_c will be $Z_v = Z_c y(Z_c)/[y_0 f(Z_c)]$, where $f(Z_c) = [y(Z_c)/Z_c] \int_0^{Z_c} dx/y(x)$. We somewhat arbitrarily, but in a fashion consistent with the existing literature, set the form of $y(Z)$ to be $y(Z) = 5.0 + 45.0[1 - \exp(-Z/B)]^{-1}$, which gives $y = 0.02$ for $Z \gg B$ and $y = 0.2$ for $Z \ll B$. Thus we have adopted a higher yield of 0.2 for metal-free stars, which may be a reasonable choice if the IMFs of metal-free stars are top heavy (Woosley & Weaver 1995). The transition metallicity B is uncertain, but we use $10^{-3}\ Z_\odot$ for the illustration (Bromm & Loeb 2003; Fang & Cen 2004).

The results reported here are based on new simulations of a *WMAP*-normalized (Spergel et al. 2003) cold dark matter model

TABLE 1
List of Simulations

Run (1)	Label (2)	Box (h^{-1} Mpc) (3)	Spatial Resolution (h^{-1} kpc) (4)	Mass Resolution ($M_\odot$) (5)	k_{max} (h Mpc^{-1}) (6)	e_{GSW} (7)
1	N432L11M	11	25	2.1×10^5	123	3×10^{-6}
2	N432L11L	11	25	2.1×10^5	123	0
3	N432L11H	11	25	2.1×10^5	123	1.5×10^{-5}
4	N864L11M	11	13	2.7×10^4	123	3×10^{-6}
5	N864L22M	22	25	2.1×10^5	123	3×10^{-6}
6	N432L11M8	11	25	2.1×10^5	31	3×10^{-6}
7	N432L11M32	11	25	2.1×10^5	7.7	3×10^{-6}

Notes.—Cols. (1) and (2): a numeric number for each run and a label indicating the number of cells used (432 for 432^3 cells and 864 for 864^3 cells), the box size (11 and 22 h^{-1} Mpc), and the level of GSW ("L" for low, "M" for median, and "H" for high). The simulations labeled with N432 have 216^3 dark matter particles, whereas those labeled with N864 have 432^3 dark matter particles. Cols. (3) and (4) : box sizes and spatial resolution, respectively, both in comoving units. Col. (5): the mean baryonic cell mass; the corresponding dark matter particle mass is 1.0×10^7 $M_\odot$ for runs 1, 2, 3, 5, 6, and 7 and 1.3×10^6 $M_\odot$ for run 4. Col. (6): initial maximum wavenumber k_{max} for the input power spectrum in comoving h Mpc^{-1}. Col. (7): the GSW strength.

with a cosmological constant: $\Omega_M = 0.29$, $\Omega_b = 0.047$, $\Omega_\Lambda = 0.71$, $\sigma_8 = 0.85$, $H_0 = 100\ h$ km s^{-1} Mpc^{-1} $= 70$ km s^{-1} Mpc^{-1}, and $n = 1.0$. Seven simulations with varying box size, resolution, and input physics are made, as listed in Table 1. Mass resolution is extremely important for an analysis of this type, as it is the lowest mass systems in relatively low-density regions that contain the stars that are most suitable for contamination of the low- and moderate-density IGM. The mass resolutions are considerably better than those of most cosmological simulations, but the spatial resolution, while significantly inferior to that obtained in both the smoothed particle hydrodynamic (SPH) and adaptive mesh refinement (AMR) schemes, is, we believe, adequate for the present purpose. The coarser spatial resolution among the listed simulations is smaller than the Jeans length of the photoionized IGM at $z = 2$–4 by a factor greater than 10 but only marginally resolves some small galaxies of total mass 10^9 $M_\odot$. But our higher resolution simulation indicates that results are not significantly affected.

The first simulation (N432L11M) is our fiducial one, with a GSW feedback that is approximately matched to observations of Lyman break galaxies. The second simulation (N432L11L) has negligible GSW, while the third simulation (N432L11H) has GSW energy that is higher than the fiducial run by a factor of 5. The higher resolution run (N864L11M) has twice as high spatial resolution but with all other physics fixed the same and is made to check the dependence of the results on the resolution and the convergence of the results on resolution. As is shown below, a proper convergence has been achieved for the problem in hand. The larger simulation (N864L22M) is made to check the dependence of the results on the box size, and as one would have expected, the 11 h^{-1} Mpc box seems adequate for the objects under investigation at high redshift. The last two simulations (N432L11M8 and N432L11M32) have the exact same input physics and resolutions as the fiducial run but with the initial power spectrum cutoff at 8 and 32 cells, respectively, instead of 2 cells in the fiducial run. These two runs were made with the purpose of isolating some of the effects due to small galaxies forming from density fluctuations of high wavenumbers.

The program used to generate synthetic Lyα forest lines here is the same one used in our previous papers (Cen et al. 1994;

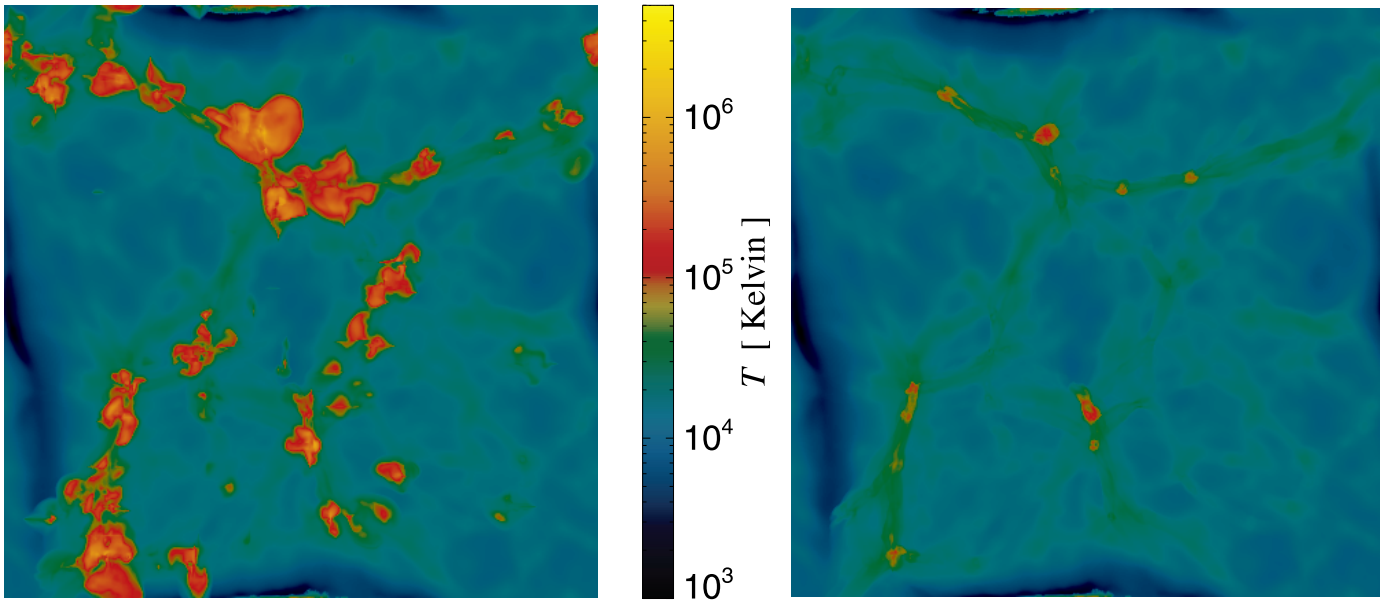

Fig. 1.—Projected temperature of a slice of size 11×11 h^{-2} Mpc^2 comoving and a depth of 2.75 h^{-1} Mpc comoving at redshift $z = 3$ with (*left*) and without (*right*) GSWs, respectively. The strength of the GSWs is normalized to LBG observations.

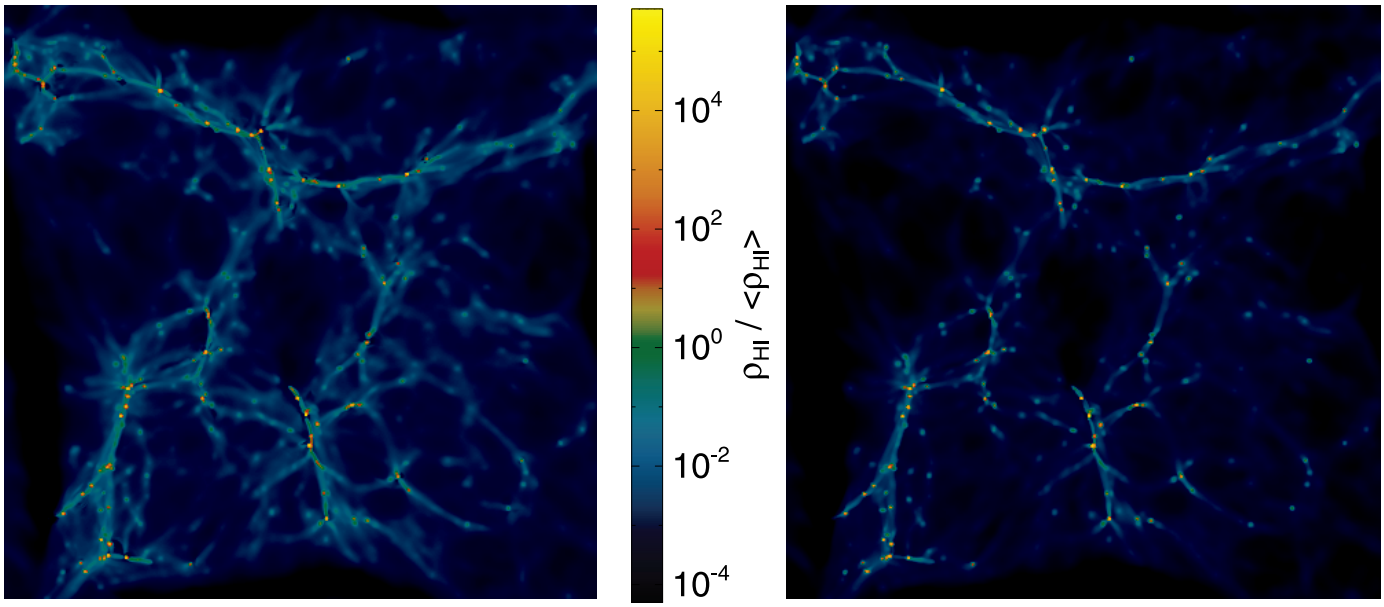

FIG. 2.—Projected neutral hydrogen overdensity of the same slice as in Fig. 1 with (*left*) and without (*right*) GSWs, respectively.

Miralda-Escudé et al. 1996). The only addition is that we have in addition the metal density, which allows detailed computations of metallicity distributions in the Lyα forest. All transmitted flux is computed with an FWHM of 6.6 km s^{-1}, a sample pixel size of 2 km s^{-1}, and Gaussian noise added to each pixel with a signal-to-noise ratio of 150. The mean decrement is chosen to match $\bar{D} = 0.34$ (e.g., Press et al. 1993) in all simulated spectra by adjusting the background radiation field to facilitate a meaningful comparison.

3. RESULTS

Figure 1 shows the distributions of IGM temperature for a typical slice of the indicated size. The left panel is with GSWs (run 1: N432L11M) and the right panel is without GSWs (run 2: N432L11L). It is clear that GSWs do blow bubbles of hot gas, which occupy a radius typically of hundreds of kiloparsecs.

Before proceeding to compute the metallicity distribution in the Lyα forest, it is pertinent to ask if a substantial GSW feedback on the IGM may spoil the excellent agreement found between the predictions of the cold dark matter model and the observed Lyα forest (Cen et al. 1994; Zhang et al. 1995; Hernquist et al. 1996; Miralda-Escudé et al. 1996; Rauch et al. 1997; Croft et al. 1999; McDonald et al. 2000). The recent work of Theuns et al. (2002) has clearly demonstrated that GSWs mainly propagate in the directions of lowest column density, and filaments (producing most of the Lyα forest) are not significantly affected by GSWs. They show quantitatively that Lyα forest statistics such as column density distribution and Doppler width distribution remain little changed, and the good agreement between cold dark matter model and observations is, to the zeroth order, unaltered by GSWs to the concerned accuracies. Here we confirm their conclusions. Figure 2 visually illustrates this point, showing little alteration of the density distributions in filaments. A joint examination of Figures 1 and 2 indicates that GSWs prefer to travel in the directions roughly perpendicular to the filaments, as found by Theuns et al. (2002).

To further demonstrate that GSWs do not significantly alter the flux distribution of the Lyα forest, Figure 3 shows the probability distributions of transmitted flux fraction, defined as $F \equiv \exp(-\tau)$, for the seven runs tabulated in Table 1. The fact that all the runs, except runs 5 (N864L22M) and 7 (N432L11M32), nearly overlay with one another clearly shows that the effect of GSWs on flux distribution and other derived quantities (such as column density distribution, etc.) will remain relatively unaltered, retaining the previous good agreement found between simulations and observations. The fact that the higher resolution run (run 4: N864L11M) agrees with lower resolution runs (runs 1, 2, and 3: N432L11M, N432L11L, and N432L11H) suggests that our fiducial run (run 1: N432L11M) has adequate resolution. The deviation of run 5 (N864L22M) from the rest is due to cosmic variance, while the deviation of run 7 (N432L11M32) from the rest is a result of missing small-scale power in that run.

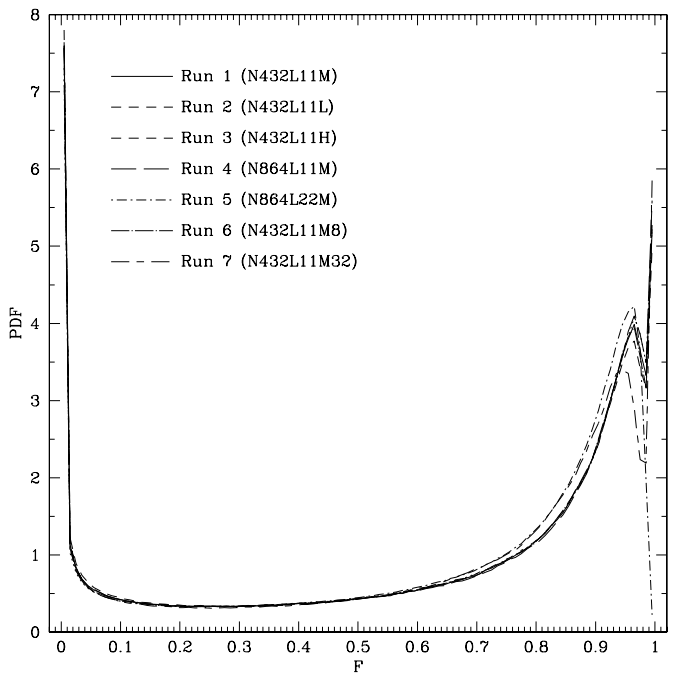

FIG. 3.—Flux probability distribution function for the seven runs at $z = 3$. [*See the electronic edition of the Journal for a color version of this figure.*]

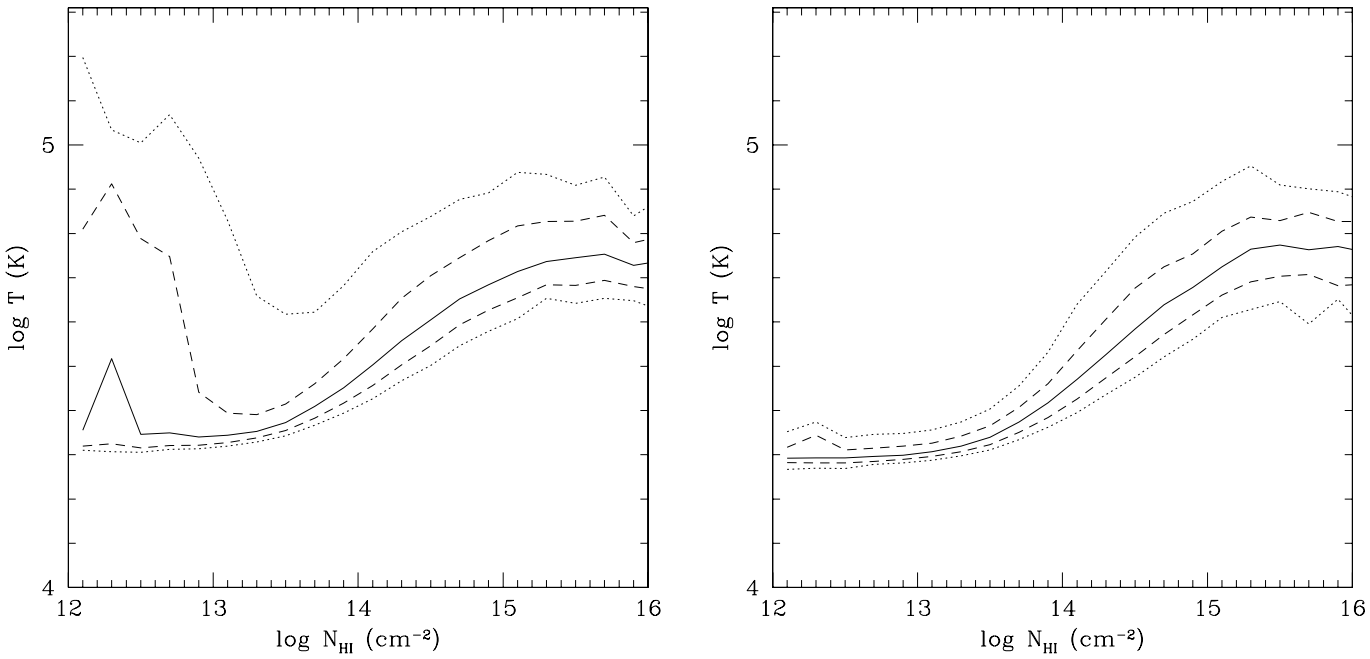

FIG. 4.—Temperature as a function of Lyα cloud column density for the two cases with (*left*; run 1: N432L11M) and without (*right*; run 2: N432L11L) GSWs, respectively, at $z = 3$. The five curves in each panel correspond to 10th, 25th, 50th, 75th, and 90th percentiles; i.e., 10% of the clouds have a temperature below the bottom curve, while 90% have a temperature below the top curve, etc. [*See the electronic edition of the Journal for a color version of this figure.*]

However, the fact that GSWs do propagate some distance, especially into the low-density regions, as shown in Figure 1, suggests that some low column density Lyα clouds should be affected to varying degrees. Figure 4 shows the temperature as a function of Lyα cloud column density for the two cases with (*left*; run 1: N432L11M) and without (*right*; run 2: N432L11L) GSWs, respectively. It is evident that, while Lyα clouds with column density $N_{\rm H\,I} \geq 10^{14}$ cm^{-2} are only affected modestly, those with $N_{\rm H\,I} \leq 10^{14}$ cm^{-2} are increasingly affected. A closer examination suggests that roughly 25% of clouds with $N_{\rm H\,I} \leq 10^{14}$ cm^{-2} are seen to experience significant heating by the GSW, and the effect decreases toward higher columns.

Let us now turn to the main point of the paper. Could the GSW transport metal-enriched gas to raise the metallicity of low-density regions to a level consistent with the observed metallicity? Are there palpable signatures of GSWs on the Lyα forest? Figure 5 shows the spatial distribution of metallicity in the IGM with (*left*) and without (*right*) GSWs. It is visible from Figure 5 that, while other, gravitational (e.g., Gnedin 1998) and hydrodynamic processes do transport metals to the vicinity ($\leq\sim$100 kpc) of galaxies without GSWs (Fig. 5, *right*), GSWs appear to play a more important role to transport the metals from galaxies to larger distances, in conjunction with other, gravitational and nongravitational processes. The "metal bubbles" (reddish

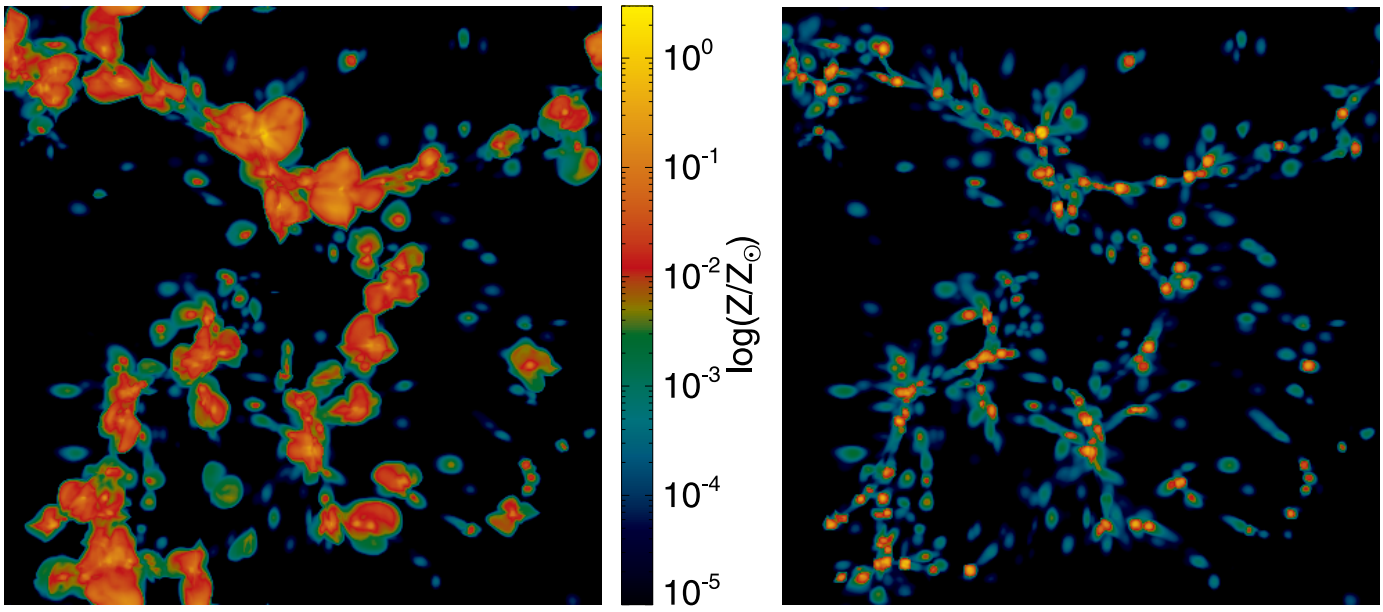

FIG. 5.—Projected metallicity of a slice of size $11 \times 11 h^{-2}$ Mpc^2 comoving and a depth of 2.75 h^{-1} Mpc comoving at redshift $z = 3$ for a *WMAP*-normalized ΛCDM model with (*left*) and without (*right*) GSWs, respectively. The strength of the GSWs is normalized to LBG observations. This is the same slice as in Fig. 1.

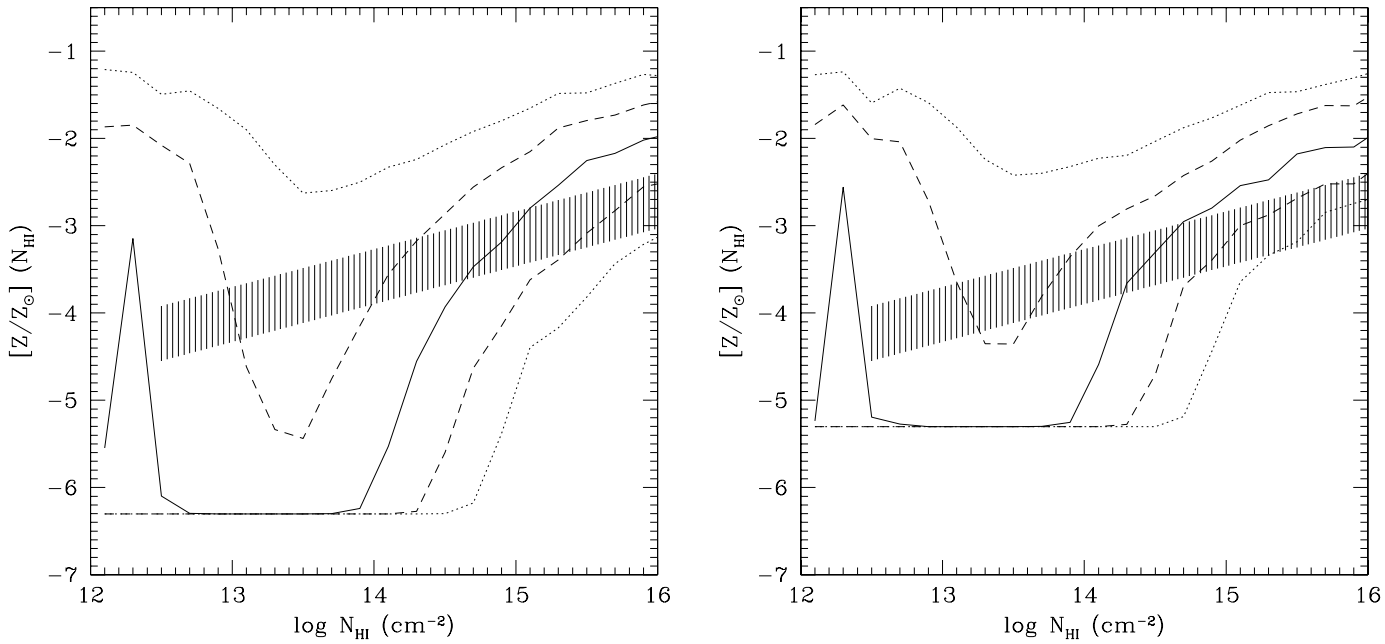

FIG. 6.—Metallicity as a function of Lyα cloud column density for run 1 (N432L11M) with two cases of metal yields: with constant yield $y_0 = 0.02$ (*left*) and with varying yield with a transition to higher yield at $Z = 10^{-3}\ Z_\odot$ (*right*), at $z = 3$. The five curves in each panel correspond to 10th, 25th, 50th, 75th, and 90th percentiles. The shaded regions indicate the observed median metallicity as a function of column density from Schaye et al. (2003) with 1 σ bounds, $[\mathrm{C/H}] = 3.47^{+0.07}_{-0.06} + 0.08^{+0.09}_{-0.07} + 0.65^{+0.10}_{-0.14}[\log(\delta) - 0.5]$, using the formula relating column density to gas density in Schaye et al. (2003), $\rho/\langle\rho\rangle = 10(N_{\mathrm{H\,I}}/10^{15}\ \mathrm{cm}^{-2})^{2/3}[(1+z)/4]^{-3}$. [*See the electronic edition of the Journal for a color version of this figure.*]

bubbles seen in the left panel of Fig. 5) have $\rho_{\mathrm{metals}}/\rho_{\mathrm{gas}} \sim 10^{-4}$, indicating that these metal-contaminated regions are enriched to a metallicity close to $10^{-2}\ Z_\odot$. But most of the volume far from galaxies remains uncontaminated by GSWs. For the runs N432L11L, N432L11M, and N432L11H the volume filling factor is 1.0%, 6.0%, and 14%, respectively, for regions with $Z > 10^{-3}\ Z_\odot$; the corresponding filling factor for regions with $Z > 10^{-2}\ Z_\odot$ is 0.28%, 4.2%, and 10% and for regions with $Z > 10^{-1}\ Z_\odot$ is 0.08%, 1.9%, and 3.6%, respectively.

Figure 6 shows the metallicity as a function of Lyα cloud column density for our fiducial run (run 1: N432L11M) with two yield schemes. For the clouds within the range of column densities ($N_{\mathrm{H\,I}} \sim 10^{14}$–$10^{15}\ \mathrm{cm}^{-2}$), for which comparisons with observations can be made, it is very encouraging that the agreement between observations and simulations is good, considering that our simulations have essentially only one free parameter for the metal yield, which in turn is fixed based on a theory of the stellar interior and turns out also to be required to match the metallicity

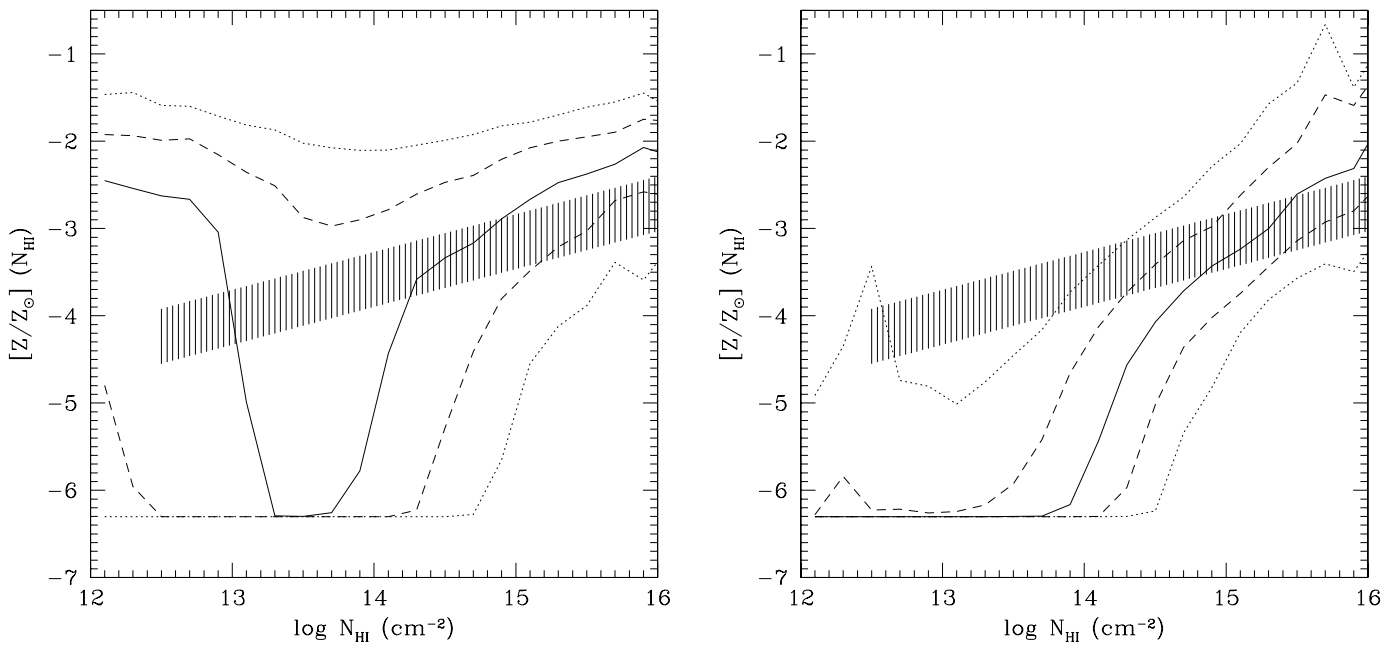

FIG. 7.—Same as Fig. 6, but for runs 3 (N432L11H, *left*) and 2 (N423L11L, *right*) with constant metal yield, at $z = 3$. [*See the electronic edition of the Journal for a color version of this figure.*]

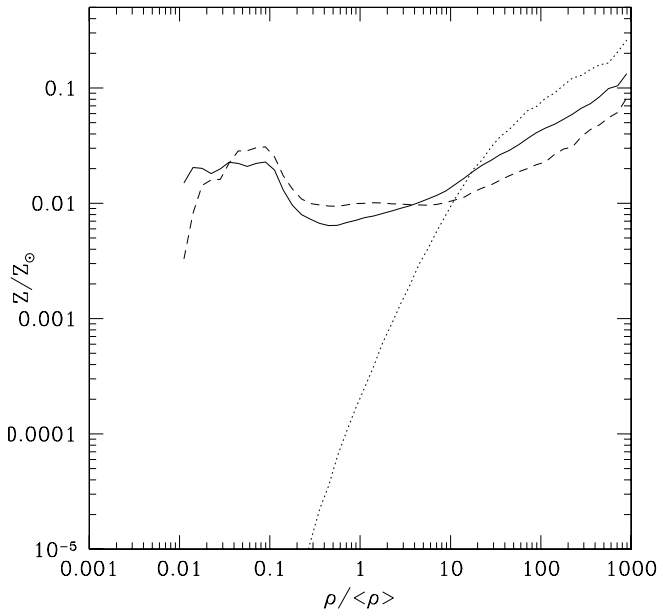

FIG. 8.—Mean metallicity as a function of gas density for three runs: fiducial with realistic GSWs (run 1: N432L11M; *solid curve*), high GSWs (run 3: N432L11H; *dashed curve*), and no GSWs (run 2: N432L11L, *dotted curve*) at $z = 3$. [*See the electronic edition of the Journal for a color version of this figure.*]

of the intracluster gas (Arnaud et al. 1994; Mushotsky et al. 1996; Mushotsky & Lowenstein 1997; Cen & Ostriker 1999b). A comparison between the left and right panels suggests that if there is a transition such that the metal yield from stars is significantly higher for nearly metal-free gas, it seems that the transition is likely to have occurred at $Z \leq 10^{-3}\ Z_\odot$, perhaps at $Z \sim 10^{-4}$ to $10^{-3}\ Z_\odot$; a transition at a higher gas metallicity would overenrich the IGM at the relevant densities.

How sensitive are the results to the strength of GSWs? Figure 7 shows the cases with GSW strength (energy) 5 times stronger than the fiducial run (*left*) and with no GSWs (*right*). We see that both these cases are consistent with observations. This is because the Lyα clouds with column densities in the range examined, where metallicity can be observationally accurately determined, are mostly located in the filaments somewhat further away from galaxies and not substantially affected by GSWs, consistent with Figure 3. This indicates the metallicity of gas in Lyα clouds with column density in the range $N_{\rm H\,I} = 10^{14.5}$–$10^{15.5}$ cm^{-2} mainly reflects the *local in situ* star formation history. Some effect of GSWs is seen in the sense that higher GSWs produce somewhat higher metallicity for the Lyα clouds in that column density range, but the differences are comparable to observational uncertainties. As it turns out, the metallicity of Lyα clouds in the column density range of $N_{\rm H\,I} = 10^{14.5}$–$10^{15.5}$ cm^{-2} provides an insensitive test of GSW (see Fig. 8 for a further demonstration).

A more powerful discriminant may lie in the metallicity of lower column density clouds, to some of which GSW are able to transport metals, as visually seen in Figures 1 and 5. A closer comparison between the left panels of Figures 6 and 7 (with GSWs) and the right panel of Figure 7 (without GSWs) already reveals this signature: *there are dramatic differences at* $N_{\rm H\,I} \leq 10^{13.5}$ cm^{-2} *between simulations with GSWs and without GSWs*, where $N_{\rm H\,I} = 10^{13.5}$ cm^{-2} approximately corresponds to $\rho/\langle\rho\rangle \leq 1$ at $z = 3$, using the formula relating column density to gas density in Schaye et al. (2003), $\rho/\langle\rho\rangle = 10(N_{\rm H\,I}/10^{15}\ {\rm cm}^{-2})^{2/3}[(1+z)/4]^{-3}$. Apparently, GSWs are able to transport metals to some low-density regions within which embedded star formation was inefficient, presumably in directions roughly perpendicular to the filaments as seen in Figures 1 and 5. In the fiducial run with GSWs (run 1: N432L11M) about 25% of Lyα clouds with $N_{\rm H\,I} < 10^{13}$ cm^{-2} may have metallicity in excess of $10^{-2}\ Z_\odot$, whereas there is none in the run without GSWs.

To elucidate this physical point, in Figure 8 we plot the mean metallicity as a function of gas density. We see the expected but now precisely quantified difference between runs with GSWs (*solid and dashed curves*) and without GSWs (*dotted curve*): GSWs are able to transport metals to regions at $\rho/\langle\rho\rangle < 10$, as expected in the hierarchical galaxy formation picture (Cen & Ostriker 1999b), whereas without GSWs most of the metals are trapped in regions with $\rho/\langle\rho\rangle > 10$. The mean metallicity is larger by factors of 7, 40, and 500 at $\rho/\langle\rho\rangle = 3,\ 1,$ and 0.1 in run 1 (N432L11M) than in run 2 (N432L11L), with the difference becoming still larger at lower $\rho/\langle\rho\rangle < 0.1$. We see that without GSWs mean metallicity is a steep monotonic function of density, whereas with GSWs there two are peaks, where the lower metallicity peak at $\rho = (0.01$–$0.1)\langle\rho\rangle$ represents metal-enriched low-density regions, a signature of GSWs, consistent with Figures 6 and 7. This is the clearest demonstration of the GSW effect on the metal enrichment of the IGM and a clear signature of GSWs: with increasing observational sensitivity one should expect to see the metallicity at lower density regions $\rho/\langle\rho\rangle < 1$ increasing rather than decreasing. The existence of a metallicity trough at $N_{\rm H\,I} = 10^{13}$–10^{14} cm^{-2} (Figs. 6 and 7) or $\rho/\langle\rho\rangle = 0.1$–1 (Fig. 8) in the simulations with GSWs is a clear indication that GSWs propagate anisotropically; in other words, some intermediate-density regions along filaments are relatively less affected. We note that metal enrichment from galaxies not resolved in our simulations (a few times $10^7\ M_\odot$) at earlier epochs is unlikely to be important compared to the observed levels, as shown by Norman et al. (2004), but may set a somewhat higher metallicity floor for the case without GSWs.

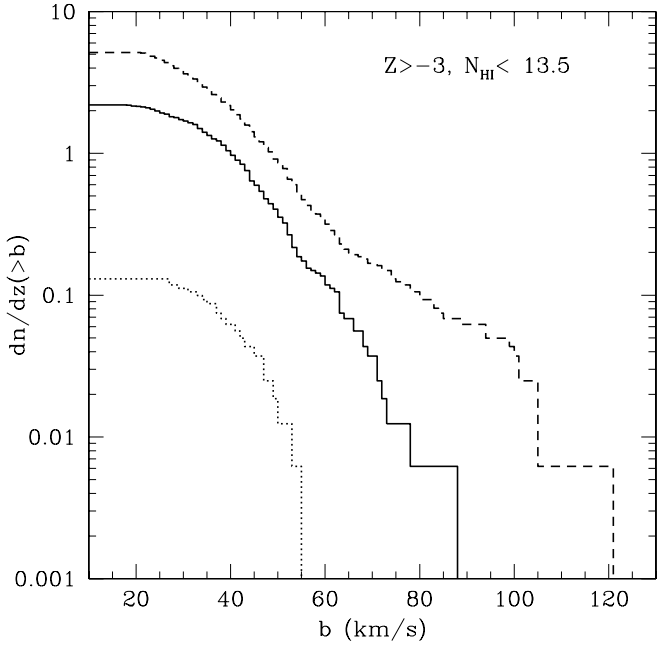

FIG. 9.—Cumulative number of Lyα cloud lines per unit redshift as a function of Doppler width, for three runs with varying GSW strengths: fiducial with realistic GSWs (run 1: N432L11M; *solid curve*), high GSWs (run 3: N432L11H; *dashed curve*), and no GSWs (run 2: N432L11L; *dotted curve*), at $z = 3$. [*See the electronic edition of the Journal for a color version of this figure.*]

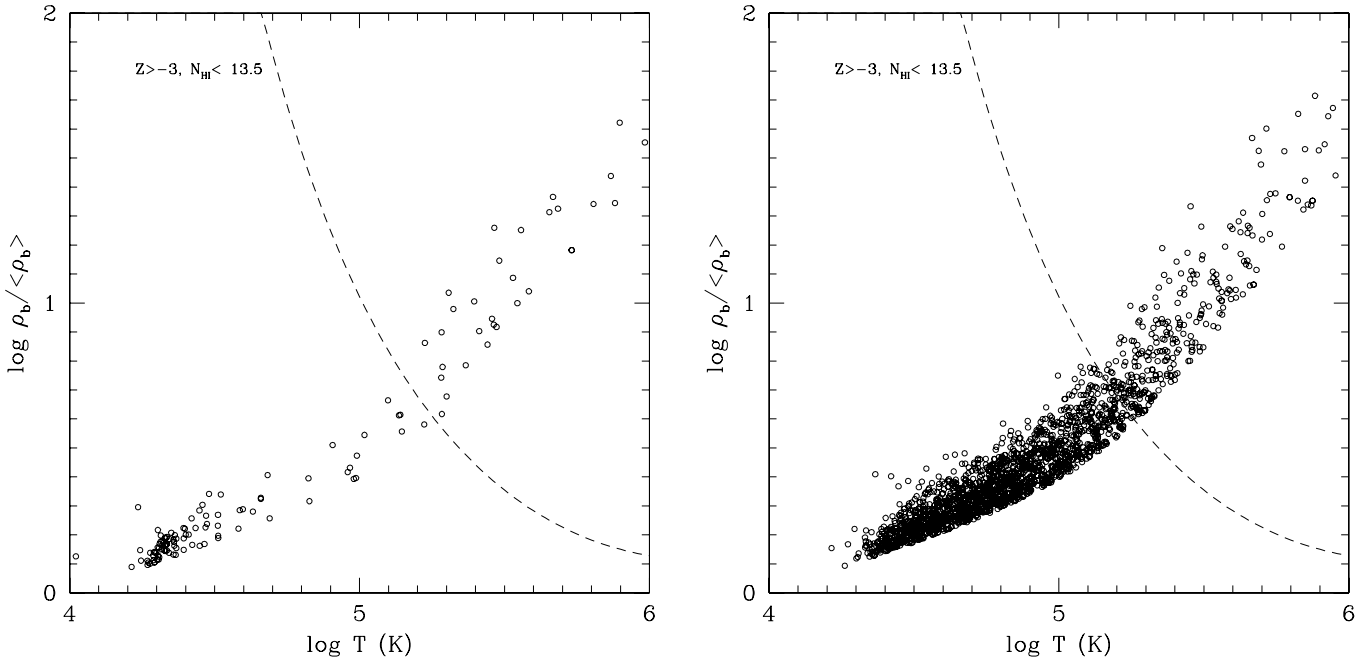

FIG. 10.—Density of Lyα clouds with $Z \geq 10^{-3}\ Z_{\odot}$ and $\log_{10}(N_{\rm H\,I}) < 13.5\ {\rm cm}^{-2}$ as a function of its temperature, for runs 2 (N432L11L, *left*) and 1 (N432L11M, *right*). The dashed curves separate photo and collisional ionization dominated regions. [*See the electronic edition of the Journal for a color version of this figure.*]

While the signature of GSWs is very visible in Figure 8, more quantitative measures are highly desirable. We have found such a measure. In Figure 9 we show the cumulative number of Lyα cloud lines with metallicity less than $10^{-3}\ Z_{\odot}$ per unit redshift as a function of Doppler width, for three runs with varying GSW strengths. It is seen that GSWs increase metal-enriched Lyα clouds at all Doppler widths at a fixed neutral column. Figure 9 may be best understood if GSWs not only propagate to low-density regions to heat up gas there to moderate temperatures, but also heat up relatively dense gas in close proximity to GSW sources to higher temperatures. In these regions the total hydrogen column density is not small, but the neutral fraction is quite small, as they have been shock-heated to $T \geq 10^5$K. In other words, those Lyα clouds with large b-values should be more highly ionized and have considerably higher total hydrogen columns. Figures 10 and 11 verify this point, showing clear correlations between density and temperature (Fig. 10) and between total hydrogen column and temperature (albeit with significant scattering; Fig. 11).

The order-of-magnitude difference in Lyα line density seen in Figure 9 between simulations with and without GSWs suggests that it could potentially provide a powerful means to measure the

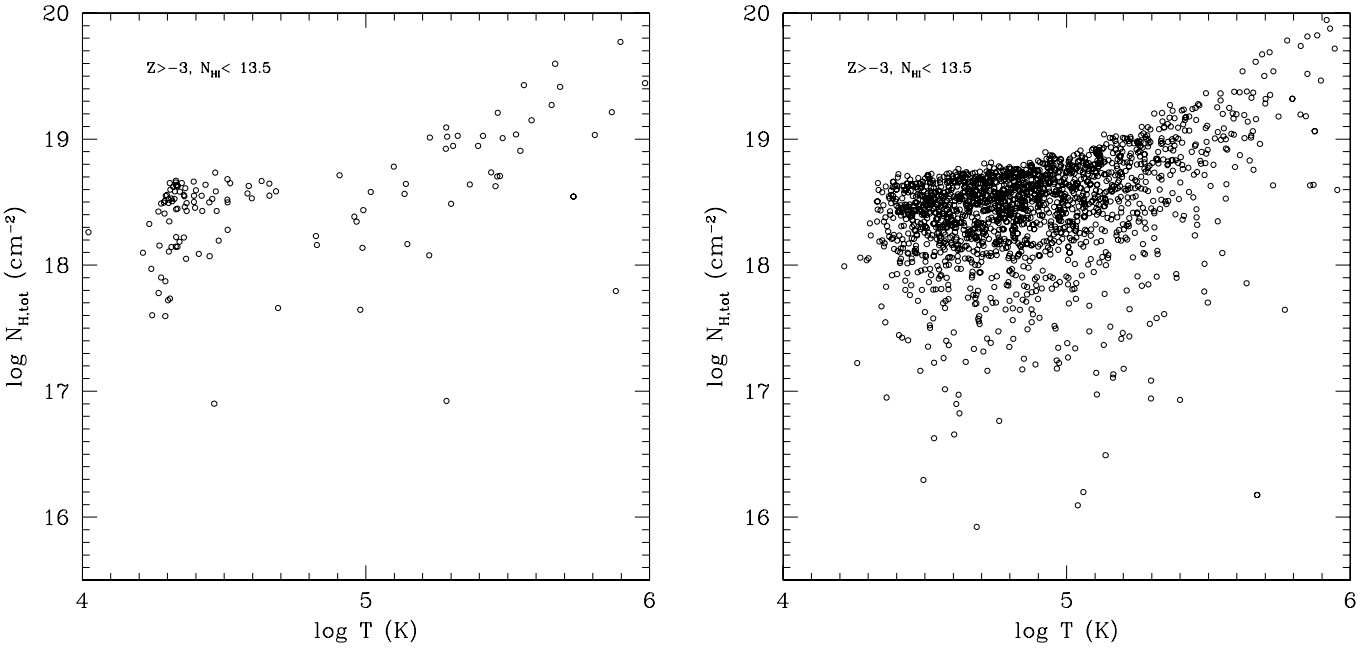

FIG. 11.—Total hydrogen column density of Lyα clouds with $Z \geq 10^{-3}\ Z_{\odot}$ and $\log_{10}(N_{\rm H\,I}) < 13.5\ {\rm cm}^{-2}$ as a function of its temperature, for runs 2 (N432L11L, *left*) and 1 (N432L11M, *right*). [*See the electronic edition of the Journal for a color version of this figure.*]

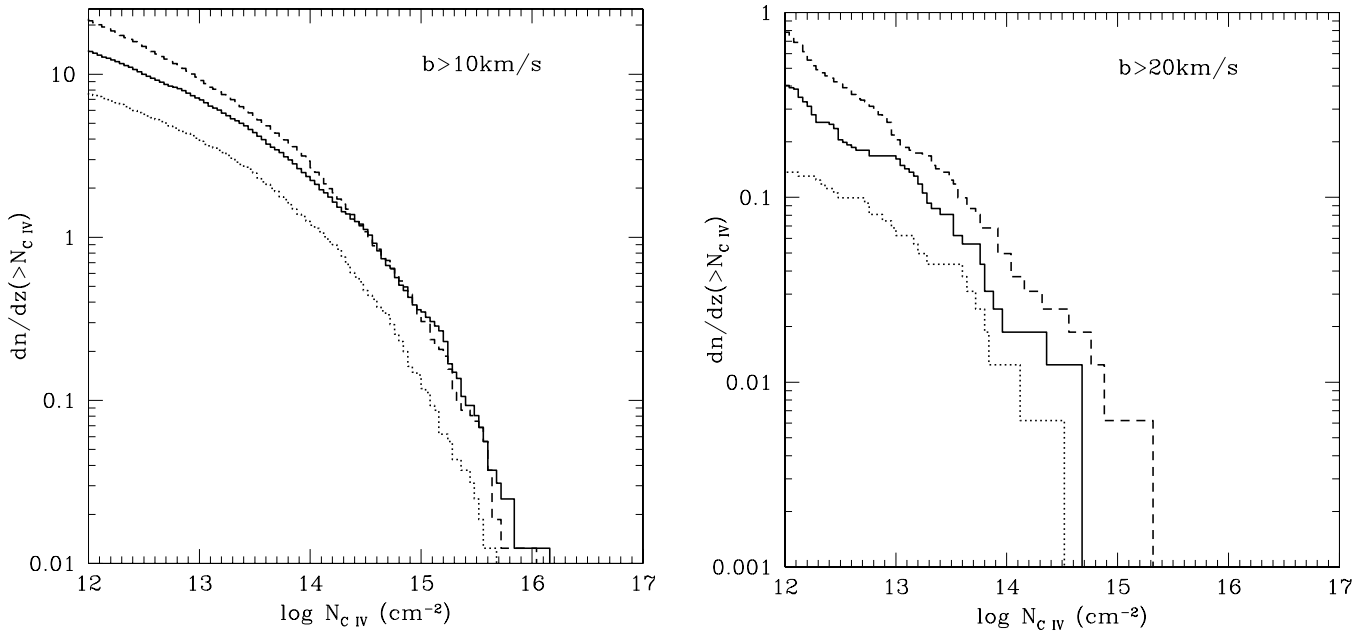

FIG. 12.—*Left*: Number of C IV lines with Doppler parameter greater than 10 km s^{-1} per unit redshift for the three runs. *Solid curve*: N432L11M; *dotted curve*: N432L11L; *dashed curve*: N432L11H. *Right*: Corresponding cases for Doppler parameter greater than 20 km s^{-1}. [*See the electronic edition of the Journal for a color version of this figure.*]

strength of GSWs. This will be an observational challenge. However, for the metal-enriched Lyα clouds, metal lines, such as the C IV and O VI lines, naturally provide the best means to detect them at the relative temperature regime. This is especially true at the high-*b* end, where such low neutral column Lyα lines may be too broad to be detectable and only metal lines may be potentially visible. We compute the expected C IV and O VI lines using the CLOUDY code (Ferland 2004), given the temperature, density, and metallicity of each cloud. Figure 12 shows the number of C IV lines with Doppler widths larger than 10 km s^{-1} per unit redshift for the three runs with varying GSW strengths, and Figure 13 the analogous plot for O VI line, including all possible clouds regardless of their metallicity. We see very substantial differences between the different runs with different GSW strengths, and the differences are larger if one selects larger width clouds. Also seen is that, while C IV lines are relatively easier to identify because it is redward of Lyα line, the O VI line appears to provide a somewhat more sensitive test of GSWs. We believe that the comparatively higher temperature regions probed by O VI line may be the primary reason for this, for which some observational evidence is emerging (e.g., Marcolini et al. 2005). We will present much more detailed analyses of metal lines and comparisons to observations in a subsequent paper. The effects of GSWs on Lyα absorption in the vicinity of Lyman break galaxies have been presented elsewhere (Kollmeier et al. 2005).

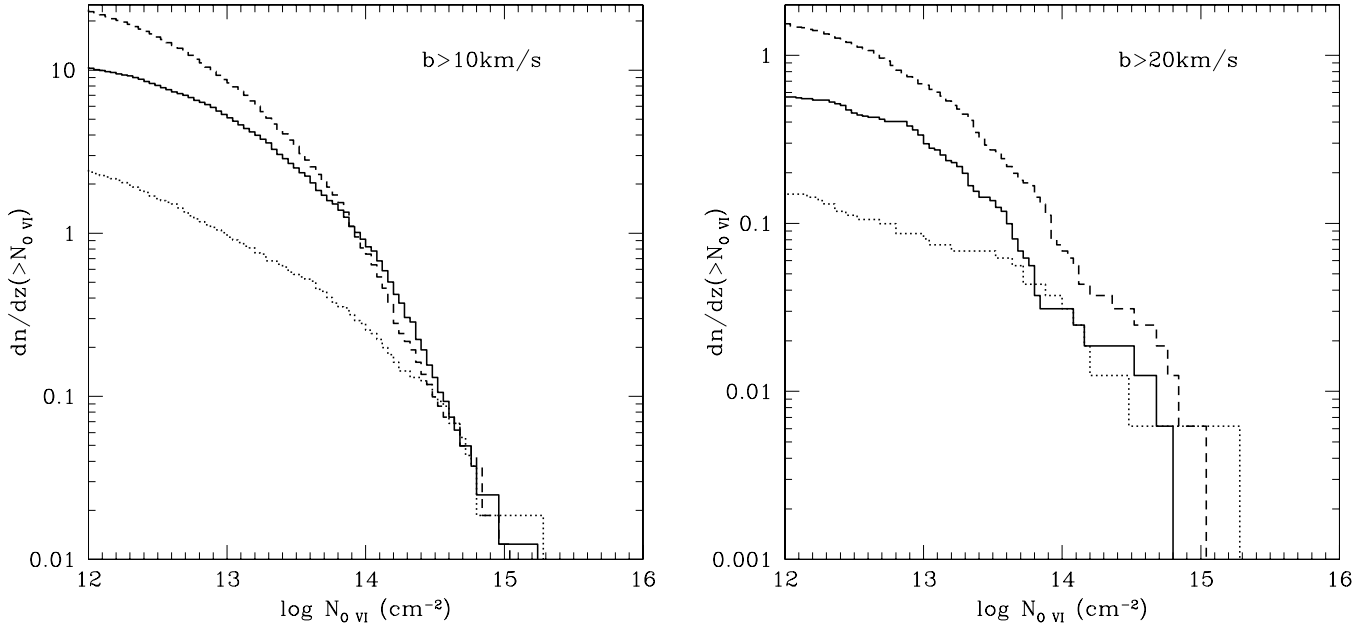

FIG. 13.—Same as Fig. 12, but for the O VI line. [*See the electronic edition of the Journal for a color version of this figure.*]

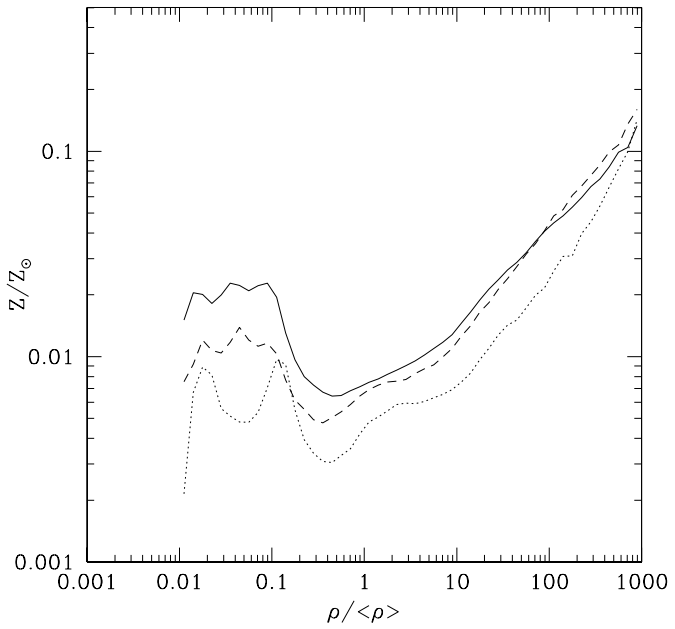

FIG. 14.—Mean metallicity as a function of gas density for three runs: fiducial run with realistic GSWs (run 1: N432L11M; *solid curve*), reduced small-scale power run at 8 cells (run 6: N432L11M8; *dashed curve*), and reduced small-scale power run at 32 cells (run 7: N432L11M32; *dotted curve*). [*See the electronic edition of the Journal for a color version of this figure.*]

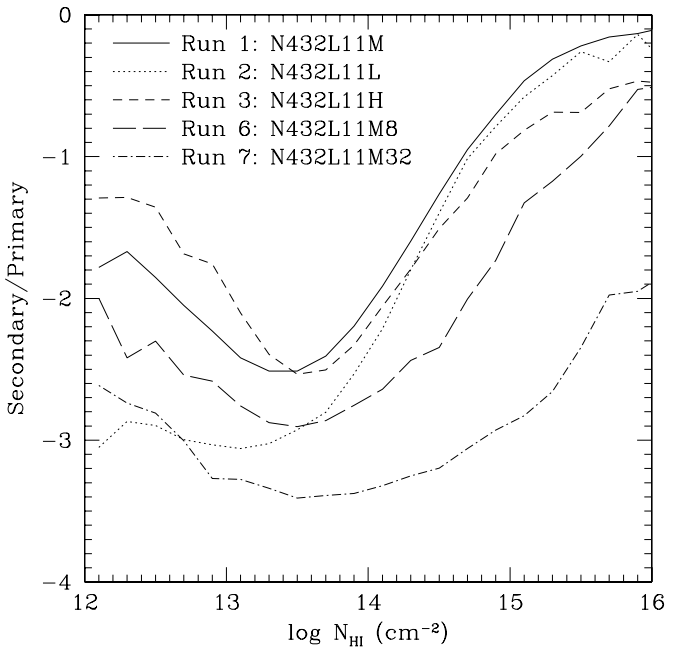

FIG. 15.—Secondary to primary metal ratio as a function of column density for five runs at $z = 3$. The units on the y-axis are relative and normalized to have the maximum of unity (normally in the densest regions). [*See the electronic edition of the Journal for a color version of this figure.*]

What galaxies are responsible for transporting metals to the low-density regions? Figure 14 shows a comparison between runs 1, 6, and 7 (N432L11M, N432L11M8, and N432L11M32). These vary in their high wavenumber cutoff, corresponding to a minimum halo mass $M_{\rm min} \sim (\pi/k_{\rm max})^3 \langle\rho\rangle$ of $1.1\times10^7\ h^{-1}\ M_\odot$, $7.0\times10^8\ h^{-1}\ M_\odot$, and $4.5\times10^{10}\ h^{-1}\ M_\odot$, in runs 1 (N432L11M), 6 (N432L11M8), and 7 (N432L11M32), respectively. We see that while the difference at $\rho/\langle\rho\rangle \sim 10^3$, where large galaxies are located, is small between the runs, the difference between runs 1 (N432L11M) and 7 (N432L11M32) is about 2.5–5.0, and the difference between runs 1 (N432L11M) and 6 (N432L11M8) is about 2 at the low-metallicity peak at $\rho/\langle\rho\rangle \sim 0.01$–$0.1$. A simple interpretation of Figure 14 is that galaxies with mass in the range 1.1×10^7–$4.5\times10^{10}\ h^{-1}\ M$ all contribute to the metal enrichment of the lower density IGM, with approximately 25% from $>4.5\times10^{10}\ h^{-1}M_\odot$, 50% from 7.0×10^8 to $4.5\times10^{10}h^{-1}M_\odot$, and 25% from $<7.0\times10^8\ h^{-1}\ M_\odot$. The recent work by Aguirre et al. (2001) has shown that massive galaxies at low redshift are not very effective in enriching the IGM to a relatively uniform degree. On the other hand, GSWs from dwarf galaxies at high redshift appear to be able to more effectively disperse metals relatively uniformly without traveling a very long distance (e.g., Schwarz et al. 1975; Cen & Bryan 2001; Madau et al. 2001). Our results are fully consistent with these earlier works. We further analyze the simulations by removing a sphere of radius $1\ h^{-1}$ Mpc around each simulated LBG, identified as galaxies brighter than rest-frame V-band magnitude $M_V = -21$, as most of the brightest galaxies in the simulation satisfy the color-color selection criteria of LBGs used by observers (e.g., Nagamine 2002; Nagamine et al. 2004, 2005). The results (not shown) in a similar plot to Figure 6 are virtually identical to Figure 6. This indicates that the contribution from ongoing star-forming massive galaxies is, as expected, negligible, simply because there is a lag due to finite GSW propagation time. This is also in part because the massive galaxies do not make large contribution to the metal enrichment of the low-density IGM, consistent with Figure 14 and earlier results of Aguirre et al. (2001).

To better understand galaxies responsible for the metal enrichment of the Lyα forest, Figure 15 shows the ratio of mean secondary metallicity to mean primary metallicity (S/P) as a function of column density. Within galaxies, the ratio of secondary to primary metals is proportional to the ratio of primary metals to hydrogen. Thus higher values of S/P indicate an origin of metals in more massive, more metal-rich systems. The most striking feature in this figure is the dramatic decrease of the ratio from $\sim$1 in the highest column density clouds to about 0.003–0.02 in the low column density clouds, a drop of a factor of 50–300, for the fiducial model (*solid curve*). Quantitatively, we see that the ratio of secondary (e.g., N) to primary metals (e.g., O, C) is expected to be smaller by a factor of 10 in clouds of $N_{\rm H\,I} \sim 10^{14.5}$ cm^{-2} compared to that in large galaxies and by a factor of $\geq$50 for $N_{\rm H\,I} \leq 10^{13.5}$ cm^{-2}. This can be most easily understood in terms that are consistent with Figure 14, if most of the metal enrichment of the Lyα forest is due to dwarf galaxies (Dekel & Silk 1986; Mac Low & Ferrara 1999; Madau et al. 2001), where gas retainment is more difficult and thus metal recycling is limited.

Some other interesting features are also present in Figure 15. A comparison among the solid, long-dashed (with GSW), and dotted (no GSW) curves reveals a couple of noticeable properties. First, the runs with GSWs show an upturn of the ratio at $N_{\rm H\,I} < 10^{13.5}$ cm^{-2}, although the level is still a factor of 50–100 below the high-density regions. The fact that there is an upturn and a valley at $N_{\rm H\,I} \sim 10^{13.5}$ cm^{-2} shows that the metals transported to the lowest density regions with $N_{\rm H\,I} < 10^{13.5}$ cm^{-2} are somewhat more recycled through stars than regions at $N_{\rm H\,I} \sim 10^{13.5}$ cm^{-2} and originate in higher metallicity systems. This may be explained if the metals are largely transported by winds from galaxies at densest peaks, where relatively more recycling has occurred, whereas near $N_{\rm H\,I} \sim 10^{13.5}$ cm^{-2} star formation and enrichment are largely local and recent. Second, increasing the

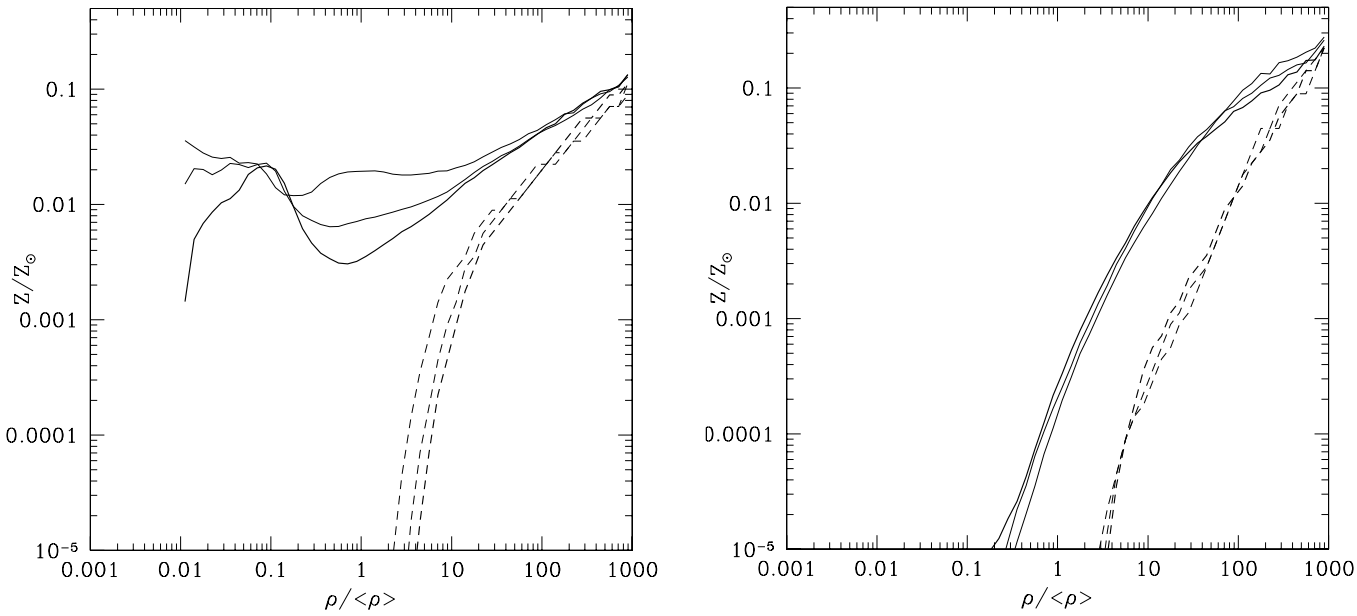

FIG. 16.—Mean metallicity (*solid curves*) and median metallicity (*dashed curves*) as a function of Lyα cloud column density at redshift $z = 2$, 3, 4 (*thick to thin lines*) for runs 1 (N432L11M; *left*) and 2 (N432L11L; *right*). [*See the electronic edition of the Journal for a color version of this figure.*]

strength of GSWs causes metals that have been more recycled to be transported to low-density regions, as expected. Comparison of the two runs with reduced small-scale power (runs 6 and 7; *long-dashed* and *dot-dashed curves*) and the fiducial run (run 1, *solid curve*) shows that the artificial removal of small-scale power, and thus low-mass galaxies, significantly reduces the overall values of the ratio of secondary to primary metals of Lyα forest concerned here, while the upturn at the low column density end is preserved. This is, of course, easily understandable, since much of previous generation of stars can no longer form without the small-scale power. This again highlights the need to have high enough $k_{\max}$ in the initial density field.

Finally, Figure 16 shows the mean and median metallicity as a function of density at three redshifts, $z = 2$, 3, 4, with GSWs (*left*) and without GSWs (*right*). Both runs show only mild evolution in the median metallicity, consistent with observations (Schaye et al. 2003): most of the contamination of the IGM was completed at a relatively high redshift. But the run with GSW shows considerable evolution for the mean metallicity at $\rho/\langle\rho\rangle < 10$, whereas the run with GSWs does not show significant evolution even for the mean metallicity at all densities.

4. CONCLUSIONS

We use the latest high–mass resolution hydrodynamic simulations of a ΛCDM model to compute the metallicity evolution of the Lyα forest. Our primary goal is to investigate possible signatures of galactic superwinds on the metallicity of the Lyα forest. There are four main points to be noted.

1. GSWs do not significantly alter the flux distribution of the Lyα forest, and the agreement found in previous simulations of a cold dark matter model with observations remains unchanged.

2. The computed metallicity of Lyα clouds in the column density range of $N_{\rm H\,I} \sim 10^{14.5}$–$10^{15.5}$ cm^{-2} at $z = 2$–4, both with and without GSWs, is in reasonable agreement with observations (Schaye et al. 2003). This suggests that these Lyα clouds do not provide a sensitive test of GSWs. On the other hand, GSWs do propagate significant distances and affect surrounding regions. The filling factor of metal-rich regions is a strong function of GSWs. With and without GSWs the volume filling factor is 6.0%, 4.2%, and 1.9% and 1.0%, 0.28%, and 0.08%, respectively, for regions with metallicity greater than 10^{-3}, 10^{-2}, and 10^{-1} $Z_\odot$.

3. We find a unique signature and sensitive test of GSWs, which lies in the still lower density regions, with a gas density of $\rho/\langle\rho\rangle = 0.01$–1.0 and a corresponding column density of $N_{\rm H\,I} \sim 10^{12}$–$10^{14}$ cm^{-2}. Without GSWs we predict that both the mean and median metallicity of Lyα clouds in this column density range at $z = 2$–4 should have $Z \leq 10^{-3}$ $Z_\odot$. With GSWs, however, there is a significant fraction (∼25%) of Lyα clouds in this column density range that have a high metallicity excess of 10^{-2} $Z_\odot$, resulting in a mean metallicity of $\sim 10^{-2}$ $Z_\odot$. Most importantly, we were able to condense all this information to a first quantitative measure of the strength of GSWs. We predict that the number of such lines per unit redshift at $z \sim 3$ should be about 0.1 in the absence of GSWs. With the observed GSW strength, we expect to see 20–50 such lines per unit redshift. This poses an observational challenge. Furthermore, we find that the difference between simulations with and without GSWs becomes much larger with regard to a subset of such clouds with high Doppler widths ($b \geq 60$ km s^{-1}). We find that the number of metal lines, such as C IV and O VI lines, per unit redshift differs significantly for different strengths of GSWs and may potentially provide the best probes for measuring GSWs.

4. If we (artificially) reduce the number of low-mass galaxies ($M \leq 4.5 \times 10^{10}$ h^{-1} $M_\odot$), the contamination of the low column density clouds by GSWs is reduced by a factor of ∼4, so it is likely that the mass and metal loss from these low-mass systems at $z > 3$ (see Dekel & Silk 1986) is the origin of the metals. There is a potential test of this hypothesis. Since the reprocessing of metals in these low-mass systems is negligible, the ratio of secondary (e.g., N) to primary metals (e.g., O, C) is very low, and indeed when we examine this tracer, we find that the ratio of secondary to primary metals is expected to be smaller by a factor of 10 and ≥50 for clouds of $N_{\rm H\,I} \sim 10^{14.5}$ and $N_{\rm H\,I} \leq 10^{13.5}$ cm^{-2},

respectively, compared to that in large galaxies. Thus, future observations of N/O or N/C would help provide an additional test of our proposal. In addition, we find that there is a minimum in the median metallicity for clouds of $N_{\rm H\,I} \sim 10^{13}$–$10^{14}$ cm^{-2} in the case with GSWs, whereas without GSWs the metallicity decreases monotonically and rapidly with decreasing column density.

We thank Taotao Fang for providing lookup tables for C IV and O VI lines using CLOUDY. We thank Len Cowie, Piero Madau, and Max Pettini for useful discussions, and an anonymous referee for a very constructive report that helped improve the paper. This work is supported in part by grants AST 02-06299, NAG5-13381, NNG05GK10G, and AST 05-07521.

REFERENCES

Adelberger, K. L. 2003, in ASP Conf. Ser. 291, Hubble's Science Legacy: Future Optical/Ultraviolet Astronomy from Space, ed. K. R. Sembach, J. C. Blades, G. D. Illingworth, & R. C. Kennicutt, Jr. (San Francisco: ASP), 221
Adelberger, K. L., Steidel, C. C., Shapley, A. E., & Pettini, M. 2003, ApJ, 584, 45
Afshordi, N., & Cen, R. 2002, ApJ, 564, 669
Aguirre, A. 1999, ApJ, 525, 583
Aguirre, A., Hernquist, L., Schaye, J., Katz, N., Weinberg, D. H., & Gardner, J. 2001, ApJ, 561, 521
Arnaud, K. A., et al. 1994, ApJ, 436, L67
Arnett, D. 1996, Supernovae and Nucleosynthesis (Princeton: Princeton Univ. Press)
Babul, A., Balogh, M. L., Lewis, G. F., & Poole, G. B. 2002, MNRAS, 330, 329
Balogh, M. L., Babul, A., & Patton, D. R. 1999, MNRAS, 307, 463
Bergeron, J., Aracil, B., Petitjean, P., & Pichon, C. 2002, A&A, 396, L11
Bertschinger, E. 2001, ApJS, 137, 1
Bialek, J. J., Evrard, A. E., & Mohr, J. J. 2001, ApJ, 555, 597
Bland, J., & Tully, B. 1988, Nature, 334, 43
Bond, J. R., & Wadsley, J. W. 1998, Structure and Evolution of the Intergalactic Medium from QSO Absorption Line System (Gif-sur-Yvette: Editions Frontières), 143
Borgani, S., Governato, F., Wadsley, J., Menci, N., Tozzi, P., Lake, G., Quinn, T., & Stadel, J. 2001, ApJ, 559, L71
Brighenti, F., & Mathews, W. G. 2001, ApJ, 553, 103
Bromm, V., & Loeb, A. 2003, Nature, 425, 812
Bruzual, A. G. 2000, preprint (astro-ph/0011094)
Bruzual, A. G., & Charlot, S. 1993, ApJ, 405, 538
Cen, R., & Bryan, G. L. 2001, ApJ, 546, L81
Cen, R., Kang, H., Ostriker, J. P., & Ryu, D. 1995, ApJ, 451, 436
Cen, R., Miralda-Escudé, J., Ostriker, J. P., & Rauch, M. 1994, ApJ, 437, L9
Cen, R., & Ostriker, J. P. 1992, ApJ, 399, L113
———. 1993, ApJ, 417, 415
———. 1999a, ApJ, 514, 1
———. 1999b, ApJ, 519, L109
Cen, R., Ostriker, J. P., Prochaska, J. X., & Wolfe, A. M. 2003, ApJ, 598, 741
Chevalier, R. A., & Clegg, A. W. 1985, Nature, 317, 44
Croft, R. A. C., Weinberg, D. H., Pettini, M., Hernquist, L., & Katz, N. 1999, ApJ, 520, 1
Dahlem, M., Weaver, K. A., & Heckman, T. M. 1998, ApJS, 118, 401
Davé, R., et al. 2001, ApJ, 552, 473
David, L. P., Forman, W., & Jones, C. 1991, ApJ, 380, 39
Dawson, S., Spinrad, H., Stern, D., Dey, A., van Breugel, W., De Vries, W., & Reuland, M. 2002, ApJ, 570, 92
Deharveng, J.-M., Buat, V., Le Brun, B., Milliard, B., Kynth, D., Shull, J. M., & Gry, C. 2001, A&A, 375, 805
Dekel, A., & Silk, J. 1986, ApJ, 303, 39
Della Ceca, R., Griffiths, R. E., Heckman, T. M., Lehnert, M. D., & Weaver, K. A. 1999, ApJ, 514, 772
Dyson, J. E., Arthur, S. J., & Hartquist, T. W. 2002, A&A, 390, 1063
Elizondo, D., Yepes, G., Kates, R., & Klypin, A. 1999a, NewA, 4, 101
Elizondo, D., Yepes, G., Kates, R., Muller, V., & Klypin, A. 1999b, ApJ, 515, 525
Fang, T., & Cen, R. 2004, ApJ, 616, L87
Fang, T., Marshall, H. L., Lee, J. C., Davis, D. S., & Canizares, C. R. 2002, ApJ, 572, L127
Ferland, G. J., Korista, K. T., Verner, D. A., Ferguson, J. W., Kingdon, J. B., & Verner, E. M. 1998, PASP, 110, 761
Ferrara, A., Pettini, M., & Shchekinov, Y. 2000, MNRAS, 319, 539
Filippenko, A. V., & Sargent, W. L. W. 1992, AJ, 103, 28
Franx, M., Illingworth, G. D., Kelson, D. D., van Gokkum, P. G., & Tran, K.-V. 1997, ApJ, 486, L75
Gnedin, N. Y. 1998, MNRAS, 294, 407
Gnedin, N. Y., & Ostriker, J. P. 1997, ApJ, 486, 581
Hartquist, T. W., Dyson, J. E., & Williams, R. J. R. 1997, ApJ, 482, 182
Heckman, T. M., 2001, in ASP Conf. Ser. 240, Gas and Galaxy Evolution, ed. J. E. Hibbard, M. Rupen, & J. H. van Gorkom (San Francisco: ASP), 345
Heckman, T. M., Armus, L., & Miley, G. K. 1987, AJ, 93, 276
Heckman, T. M., Robert, C., Leitherer, C., Garnett, D. R., & van der Rydt, F. 1998, ApJ, 503, 646
Heckman, T. M., Sembach, K. R., Meurer, G. R., Leitherer, C., Calzetti, D., & Martin, C. L. 2001, ApJ, 558, 56
Hernquist, L., Katz, N., Weinberg, D. H., & Miralda-Escudé, J. 1996, ApJ, 457, L51
Hultman, J., & Pharasyn, A. 1999, A&A, 347, 769
Hurwitz, M., Jelinsky, P., & Dixon, W. V. D. 1997, ApJ, 481, L31
Kaiser, N. 1991, ApJ, 383, 104
Katz, N., Hernquist, L., & Weinberg, D. H. 1992, ApJ, 399, L109
———. 1996, ApJS, 105, 19
Kay, S. T., Pearce, F. R., Frenk, C. S., & Jenkins, A. 2002, MNRAS, 330, 113
Kollmeier, J. A., Miralda-Escudé, J., Cen, R., & Ostriker, J. P. 2005, ApJ, in press (astro-ph/0503674)
Koo, B.-C., & McKee, C. F. 1992a, ApJ, 388, 93
———. 1992b, ApJ, 388, 103
Lehnert, M. D., & Heckman, T. M. 1996, ApJ, 462, 651
Lloyd-Davies, E. J., Ponman, T. J., & Cannon, D. B. 2000, MNRAS, 315, 689
Loewenstein, M. 2000, ApJ, 532, 17
Mac Low, M.-M., & Ferrara, A. 1999, ApJ, 513, 142
Madau, P., Ferrara, A., & Rees, M. J. 2001, ApJ, 555, 92
Marcolini, A., Strickland, D. K., D'Ercole, A., Heckman, T. M., & Hoopes, C. G. 2005, MNRAS, 362, 626
Marlowe, A. T., Heckman, T. M., Wyse, R. F. G., & Schommer, R. 1995, ApJ, 438, 563
Martin, C. L. 1999, ApJ, 513, 156
Martin, C. L., Kobulnicky, H. A., & Heckman, T. M. 2002, ApJ, 574, 663
Mathur, S., Weinberg, D. H., & Chen, X. 2003, ApJ, 582, 82
McCarthy, I. G., Babul, A., & Balogh, M. L. 2002, ApJ, 573, 515
McCarthy, P. J., Heckman, T. M., & van Breugel, W. 1987, AJ, 93, 264
McDonald, P., Miralda-Escudé, J., Rauch, M., Sargent, W. L. W., Barlow, T. A., Cen, R., & Ostriker, J. P. 2000, ApJ, 543, 1
McKee, C. F., & Ostriker, J. P. 1977, ApJ, 218, 148
Metzler, C. A., & Evrard, A. E. 1994, ApJ, 437, 564
Miralda-Escudé, J., Cen, R., Ostriker, J. P., & Rauch, M. 1996, ApJ, 471, 582
Mori, M., Ferrara, A., & Madau, P. 2002, ApJ, 571, 40
Mushotzky, R. F., & Lowenstein, M. 1997, ApJ, 481, L63
Mushotzky, R. F., Lowenstein, M., Arnaud, A. K., Tamura, T., Fukazawa, Y., Matsushita, K., Kikuchi, K., & Hatsukade, I. 1996, ApJ, 466, 686
Nagamine, K. 2002, ApJ, 564, 73
Nagamine, K., Cen, R., Hernquist, L., Ostriker, J. P., & Springel, V. 2005, ApJ, 618, 23
Nagamine, K., Springel, V., Hernquist, L., & Machacek, M. 2004, MNRAS, 350, 385
Nath, B. B., & Trentham, M. 1997, MNRAS, 291, 505
Navarro, J. F., Frenk, C. S., & White, S. D. M. 1995, MNRAS, 275, 720
Neumann, D. M., & Arnaud, M. 2001, A&A, 373, L33
Nicastro, F., et al. 2002, ApJ, 573, 157
Norman, M. L., O'Shea, B. W., & Paschos, P. 2004, ApJ, 601, L115
Ostriker, J. P., & Cowie, L. L. 1981, ApJ, 243, L127
Papaderos, P., Fricke, K. J., Thuan, T. X., & Loose, H.-H. 1994, A&A, 291, L13
Pen, U.-L. 1999, ApJ, 510, L1
Pettini, M., Kellogg, M., Steidel, C. C., Dickinson, M., Adelberger, K. L., & Giavalisco, M. 1998, ApJ, 508, 539
Pettini, M., Rix, S. A., Steidel, C. C., Adelberger, K. L., Hunt, M. P., & Shapley, A. E. 2002, ApJ, 569, 742
Pettini, M., Shapley, A. E., Steidel, C. C., Cuby, J.-G., Dickinson, M., Moorwood, A. F. M., Adelberger, K. L., & Giavalisco, M. 2001, ApJ, 554, 981
Ponman, T. J., Cannon, D. B., & Navarro, J. F. 1999, Nature, 397, 135
Press, W. H., Rybicki, G. B., & Schneider, D. P. 1993, ApJ, 414, 64
Rauch, M., et al. 1997, ApJ, 489, 7
Raymond, J. C., Cox, D. P., & Smith, B. W. 1976, ApJ, 204, 290
Ricotti, M., & Ostriker, J. P. 2004, MNRAS, 350, 539
Ritchie, B. W., & Thomas, P. A. 2001, MNRAS, 323, 743
Rupke, D. S., Veilleux, S., & Sanders, D. B. 2002, ApJ, 570, 588
Ryu, D., Ostriker, J. P., Kang, H., & Cen, R. 1993, ApJ, 414, 1
Sazonov, S. Y., Ostriker, J. P., & Sunyaev, R. A. 2004, MNRAS, 347, 144

Scannapieco, E., Ferrara, A., & Madau, P. 2002, ApJ, 574, 590
Scannapieco, E., Thacker, R. J., & Davis, M. 2001, ApJ, 557, 605
Schaye, J., Aguirre, A., Kim, T.-S., Theuns, T., Rauch, M., & Wallace, W. L. W. 2003, ApJ, 596, 768
Schwarz, J., Ostriker, J. P., & Yahil, A. 1975, ApJ, 202, 1
Smith, S. J. 1996, ApJ, 473, 773
Songaila, A., & Cowie, L. L. 1996, AJ, 112, 335 (SC96)
Spergel, D. N., et al. 2003, ApJS, 148, 175
Springel, V., & Hernquist, L. 2003, MNRAS, 339, 289
Steinmetz, M. 1996, MNRAS, 278, 1005
Strickland, D. K., & Stevens, I. R. 2000, MNRAS, 314, 511
Suchkov, A. A., Berman, V. G., Heckman, T. M., & Balsara, D. S. 1996, ApJ, 463, 528
Thacker, R. J., Scannapieco, E., & Davis, M. 2002, ApJ, 581, 836
Theuns, T., Leonard, A., Efstathiou, G., Pearce, F. R., & Thomas, P. R. 1998, MNRAS, 301, 478
Theuns, T. T., Viel, M., Kay, S., Schaye, J., Carswell, R. F., & Tzanavaris, P. 2002, ApJ, 578, L5
Tozzi, P., & Norman, C. 2001, ApJ, 546, 63
Tripp, T. M., Savage, B. D., & Jenkins, E. B. 2000, ApJ, 534, L1
Tytler, D., Fan, X.-M., Burles, S., Cottrell, L., Davis, C., Kirkman, D., & Zuo, L. 1995, in QSO Absorption Lines, ed. G. Meylan (Berlin: Springer), 289
Veilleux, S., Bland-Hawthorn, J., Cecil, G., Tully, R. B., & Miller, S. T. 1999, ApJ, 520, 111
Veilleux, S., Shopbell, P. L., & Miller, S. T. 2001, AJ, 121, 198
Voit, G. M., & Bryan, G. L. 2001, Nature, 414, 425
Voit, G. M., Bryan, G. L., Balogh, M. L., & Bower, R. G. 2002, ApJ, 576, 601
White, M., Hernquist, L., & Springel, V. 2002, ApJ, 579, 16
White, R. E., III. 1991, ApJ, 367, 69
Woosley, S. E., & Weaver, T. A. 1995, ApJS, 101, 181
Wu, K. K. S., Fabian, A. C., & Nulsen, P. E. J. 2000, MNRAS, 318, 889
Yepes, G., Kates, R., Khokhlov, A., & Klypin, A. 1997, MNRAS, 284, 235
Yoshida, M., Taniguchi, Y., & Murayama, T. 1999, AJ, 117, 1158
Zhang, Y., Anninos, P., & Norman, M. L. 1995, ApJ, 453, L57